

# The projected stellar mass distribution and the transition to homogeneity

José Gaite\*

Physics Dept., ETSIAE, Univ. Politécnica de Madrid, E-28040 Madrid, Spain

January 14, 2020

## ABSTRACT

We make a statistical analysis of the angular projection of the large-scale stellar mass distribution, obtained from the Sloan Digital Sky Survey (data release 7) with the stellar masses of galaxies. We obtain a clustering length  $r_0 = 5.9\text{--}6.5 h^{-1}\text{Mpc}$  and a two-point correlation function power-law exponent  $\gamma = 1.83\text{--}1.97$ , but we find that the projected stellar mass distribution is not very useful to study strong clustering and, in particular, fractal properties. Taking into account the results of the statistical analysis of volume limited samples from the same data, we conclude that a multifractal cosmic-web model with a transition to homogeneity at about  $10 h^{-1}\text{Mpc}$  is adequate, but there is a considerable uncertainty in both this scale and the correlation dimension.

**Key words.** cosmology: large-scale structure of Universe – galaxies: clusters: general – methods: statistical

## 1. Introduction

It is claimed that we are entering the era of precision cosmology, in which the fundamental parameters of the universe are known within a few percent precision and only remains to progressively refine them (Jones 2017; Lahav and Liddle 2017). In addition to the global parameters of the FLRW model, we have the parameters that determine the primordial density perturbations and hence the formation of large scale structure; in particular, the amplitude of the primordial density perturbations, usually measured in terms of the present linear-theory mass dispersion on a scale of  $8 h^{-1}\text{Mpc}$ , named  $\sigma_8$ . The scale of  $8 h^{-1}\text{Mpc}$  comes from Peebles' observation that galaxy counts on this scale have a rms fluctuation approximately equal to one (Peebles 1993). In general, the mass dispersion over the length  $R$ ,  $\sigma(R)$ , defines a scale such that  $\sigma(R) = 1$ , which separates the strong clustering regime from the large-scale quasi-homogeneous mass distribution.

A similar scale is the clustering length of galaxies  $r_0$ , such that  $\xi(r_0) = 1$ , where  $\xi(r)$  is the reduced galaxy-galaxy correlation function. This function is well approximated by the power law

$$\xi(r) = \left(\frac{r_0}{r}\right)^\gamma, \quad (1)$$

for distances not much larger than  $r_0$  (Peebles 1993). The scale such that the rms dispersion of galaxy counts is equal to one is related to  $r_0$  by a  $\gamma$ -dependent factor (Peebles 1993). Historically, the power-law form of  $\xi(r)$  was deduced from the *angular* positions of galaxies, yielding  $\gamma = 1.8$  and  $r_0 = 4.7 h^{-1}\text{Mpc}$  (Totsuji and Kihara 1969; Groth and Peebles 1977). Nowadays, in spite of the availability of galaxy redshift surveys, the angular positions are

still useful, because they are more precise and more abundant than the radial positions, allowing better statistics. In particular, the angular correlation function  $w(\theta)$  is used, in combination with other data, for recent precision values of  $\sigma_8$  (Lahav and Liddle 2017; DES Collaboration 2018). The study of the Sloan Digital Sky Survey presented here also shows that the angular positions allow better statistics and longer scaling ranges than volume-limited redshift samples.

The amplitude of the primordial density perturbations is not theoretically constrained and determines the present scale of transition to homogeneity. The transition to homogeneity has been the subject of numerous studies, many of them motivated by the bold proposal that no such transition exists (Mandelbrot 1983; Pietronero 1987; Coleman and Pietronero 1992). This proposal, namely, that the mass distribution is fully scale invariant, at all scales in a Newtonian cosmology, has been called the “fractal universe” (Peebles 1993); which is quite a misnomer, because fractal geometry is defined to describe the properties of mass distributions on small rather than large scales. Indeed, Eq. (1) corresponds to a fractal distribution on scales  $r \ll r_0$ , for any magnitude of  $r_0$ . This scale, or any suitable scale of transition to homogeneity, separates the quasi-homogeneous or linear regime of the evolution of density fluctuations from the strong clustering or nonlinear regime, to which fractal geometry applies.

The scale and form of the transition to homogeneity determine the size of the largest structures that can be observed (Gaite, Domínguez and Pérez-Mercader 1999). An examination of the literature shows values of the scale of transition to homogeneity that go from  $5 h^{-1}\text{Mpc}$  to more than  $20 h^{-1}\text{Mpc}$  (Peebles 1993; Jones et al. 2004; Sylos Labini, Vasiliev and Baryshev 2007; Sarkar et al. 2009; Verevkin, Bukhmastova and Baryshev 2011; Chacón-Cardona et al. 2016). In contrast, the current precision values of  $\sigma_8$  are assigned a relative error of about

\* E-mail: jose.gaite@upm.es

one percent (Lahav and Liddle 2017). This precision is surprisingly good, in comparison with the low precision of the present scale of transition to homogeneity, which is a scale determined by  $\sigma_8$ .

For its intrinsic interest and for its application to the study of the transition to homogeneity, we make a new analysis of angular correlations, adding an important ingredient: the stellar masses of galaxies. To be precise, we are going to study the angular projection of the stellar mass distribution. The distribution of stellar mass has already been studied by Li and White (2009), employing the projected correlation function  $w(r_p)$ , on scales  $r_p < 30 h^{-1}\text{Mpc}$  [ $r_p$  is the separation perpendicular to the line of sight (Davis and Peebles 1983)]. Li and White find that the  $w(r_p)$  of stellar mass is very well represented, over the range  $10 h^{-1}\text{kpc} < r_p < 10 h^{-1}\text{Mpc}$ , by a power law such that  $\gamma = 1.84$  and  $r_0 = 6.1 h^{-1}\text{Mpc}$  in Eq. (1). Li and White compare the scalings of the stellar mass and galaxy distributions and find that the former is better.

One must be aware that the “projection” that produces  $w(r_p)$  is performed on the correlation function  $\xi(r)$  and is not associated to an actual projected distribution but to a set of local orthogonal projections on the tangent planes to the surface of the unit sphere (a rather unwieldy construction from the mathematical standpoint). The function  $w(r_p)$  depends on the length scale  $r_p$ , so it is not totally independent of redshift distortions, because there is no way to measure distances in galaxy catalogs without using the galaxy redshifts. Furthermore,  $w(r_p)$ , unlike  $\xi(r)$  or  $w(\theta)$ , is a dimensional function that does not lend itself to a straightforward interpretation. Arguably, the direct study of the angular projection of the stellar mass distribution is preferable.

As regards the importance of galaxy masses, Pietronero (1987) argued that they are necessary to study the structure of galaxy clustering. Pietronero (1987) further argued that a full *multifractal* analysis of this structure is necessary. Such analysis was initiated by Pietronero and collaborators (Coleman and Pietronero 1992; Sylos Labini, Montuori and Pietronero 1998), who estimated the masses of galaxies from the observed luminosities by assuming a simple mass-luminosity relation (a power law). Meanwhile, the large-scale structure has been known to consist not just of clusters but of a *web structure* (Geller and Huchra 1989; Kofman et al. 1992), which can be well described as a multifractal (Gaite 2018, 2019). Most of the multifractal structure is preserved in a projection, as we shall see, so it is worth studying the angular projection of the stellar mass distribution. Pietronero (1987) already considered some properties of the angular projection of a fractal galaxy distribution, and this question was further studied by Coleman and Pietronero (1992) and Durrer et al. (1997).

Our galaxy data come from the Sloan Digital Sky Survey, data release 7 (SDSS DR7) (Abazajian et al. 2009), as provided by the New York University Value-Added Galaxy Catalog (NYU-VAGC) (Blanton et al. 2005). The NYU-VAGC contains the stellar masses of the galaxies, estimated with the method described by Blanton and Roweis (2007) (which gives similar results to the method of Kauffmann et al. 2003). In fact, we use the same data as Li and White (2009), which facilitates the comparison of the respective results. Moreover, the SDSS DR7

is well studied and, in particular, there is a careful analysis of its galaxy-galaxy angular correlation function (Wang, Brunner and Dolence 2013), to which we also compare. Finally, we have recently employed the same data for a multifractal analysis of the stellar mass distribution, using volume-limited samples, and we have obtained information of the scaling properties (Gaite 2018).

Our plan is as follows. We begin in Sect. 2 with a short discussion of fractal scaling and homogeneity in galaxy redshift surveys and a re-analysis of the second statistical moment of the stellar mass coarse-grained density and its scaling with the coarse-graining length, which has been found by Gaite (2018). Then, we proceed to our main subject, namely, the properties of projections of fractal distributions, showing the relevance of the second statistical moment of the coarse-grained density of the angular projection of the stellar mass distribution (Sect. 3). We connect with the standard theory of the angular two-point correlation function of galaxies, to reinterpret it in terms of the projected mass distribution (Sect. 4). After this theoretical study, we can undertake the analysis of the angular projection of the SDSS DR7 (Sect. 5). The introduction of galaxy masses causes an unexpected problem, with which we deal in Sects. 5.2 and 5.3. In Sect. 5.4 we obtain  $r_0$  from the variance of the coarse-grained angular density. Fractional statistical moments of the coarse-grained angular density are considered in Sect. 6. We end with a general discussion (Sect. 7).

## 2. Fractal scaling and homogeneity in redshift surveys

Let us begin with some general considerations about scaling and homogeneity in redshift surveys, and, in particular, let us consider how to calculate the scale of the transition to homogeneity.

To extract directly three-dimensional information from galaxy redshift surveys, it is necessary to construct volume limited samples. If a volume limited sample is sufficiently deep, it must be possible to obtain the scale of homogeneity from it. The magnitude of the scale of homogeneity should not affect the fractal properties of the distribution of galaxies, because fractal properties are characteristic of the strongly inhomogeneous regime; but the value of the scale of homogeneity is actually necessary for an accurate calculation of, e.g., the multifractal spectrum (Gaite 2018). In fractal geometry, the multifractal spectrum  $f(\alpha)$  is a basic function that represents how mass concentrates, in terms of the number of mass concentrations of a given “strength”, measured by the *local dimension*  $\alpha$ . The function  $f(\alpha)$  is in correspondence with the *Rényi dimension* spectrum  $D_q$ , which is obtained from the scaling of statistical moments of the coarse-grained density. The scale of homogeneity is, in principle, independent of any fractal property and can be determined by evaluating the coarse-grained mass fluctuation  $(\delta M/M)(R)$ , namely, the scale dependent rms fluctuation of the stellar mass in a volume of linear dimension  $R$ , and then finding the value of  $R$  that gives an appropriate value of  $\delta M/M$ . Let us review this question.

We have recalled above Peebles’ use of the scale-dependent rms fluctuation of galaxy counts  $(\delta N/N)(R)$ , where  $N$  is the number of galaxies in a volume of linear dimension  $R$ . But it is more appropriate to consider

$(\delta M/M)(R)$ , replacing galaxy counts by total stellar mass. Therefore, to choose a definite scale of *transition* to homogeneity, it seems natural to take  $(\delta M/M)(R) = 1$ . However, one must be aware that a mass distribution with such mass fluctuations cannot be Gaussian and is not homogeneous at all. In fact, Gaite (2018) argues that a suitable criterion for homogeneity is the mass variance  $(\delta M/M)^2(R) = 0.1$ . Whether or not the scale so determined is close to the scale defined by  $\delta M/M = 1$  depends on how sharp the transition to homogeneity is; and it may not be sharp.

In this regard, it is useful to consider the precise form of the function  $(\delta M/M)(R)$ . If the two-point correlation function of the stellar mass distribution follows a power law, Eq. (1), so does  $(\delta M/M)(R)$ ; namely,

$$\frac{\delta M}{M} = C(\gamma)^{1/2} \left(\frac{r_0}{R}\right)^{\gamma/2}, \quad (2)$$

where the form of the function  $C(\gamma)$  depends on the shape of the cell. For a sphere of radius  $R$ , it is given by Peebles (1993) and fulfills  $C(\gamma)^{1/2} \in (1.1, 1.5)$  for  $\gamma \in (1, 2)$  (the normal range). Therefore, the scale such that  $\delta M/M$  equals a given number is a definite function of  $\gamma$ . For  $\delta M/M = 1$ ,  $R$  is only a little larger than  $r_0$ , whereas, for  $\delta M/M = 0.1^{1/2} = 0.32$ , it is between  $4.7r_0$  and  $12r_0$  (the larger, the smaller is  $\gamma$ ). In conclusion,  $r_0$  and the scale such that  $\delta M/M = 1$  are roughly equivalent scales but the scale where one can observe homogeneity is several times larger, especially, for low values of  $\gamma$ . The standard values  $r_0 = 5.4 h^{-1} \text{Mpc}$  and  $\gamma = 1.8$  are thus compatible with the presence of relatively large structures; for example, cosmic voids of size  $\simeq 30 h^{-1} \text{Mpc}$  (Peebles 1993). Actually, even larger structures can be observed, provided that  $\xi(r)$  does not fall too rapidly for  $r \gg r_0$  (Gaite, Domínguez and Pérez-Mercader 1999).

At any rate, the values of  $r_0$  and  $\gamma$  obtained from redshift surveys may not be precise, because the scaling range in which Eq. (1) is measured is necessarily small. Notice, for example, the broad range of values of the correlation dimension,  $D_2 = 3 - \gamma$ , namely,  $D_2 \in (1.15, 2.2)$ , when taken from various sources (Jones et al. 2004, table I). Since Eq. (1) is obtained from a linear fit of a log-log graph that yields both  $\gamma$  and  $r_0$ , the range of values of  $r_0$  has a similar breadth. In fact, one sees in the literature values of the scale of homogeneity that go from  $5 h^{-1} \text{Mpc}$  to  $30 h^{-1} \text{Mpc}$  or more (Sylos Labini, Vasilyev and Baryshev 2007; Sarkar et al. 2009; Verevkin, Bukhmastova and Baryshev 2011; Chacón-Cardona et al. 2016). Of course, some of these references are not calculating  $r_0$  but some related homogeneity scale that is necessarily larger. Chiefly, there are two common ways of defining a homogeneity scale in terms of the two-point correlation function, which can give quite different results. One can employ a power-law fit of the reduced two-point correlation function

$$\xi(r) = \frac{\langle \varrho(\mathbf{r}) \varrho(\mathbf{0}) \rangle}{\langle \varrho \rangle^2} - 1 = \frac{\langle \delta \varrho(\mathbf{r}) \delta \varrho(\mathbf{0}) \rangle}{\langle \varrho \rangle^2}, \quad (3)$$

as in Eq. (1), or a power-law fit of just the plain two-point correlation function  $\xi(r) + 1$ . Here,  $\varrho$  can be either the number density of points (galaxies) or the (stellar) mass density. If  $\xi \gg 1$ , then  $\xi$  and  $\xi + 1$  are equivalent, but this condition is not fulfilled in the full range to fit. Let us illustrate this point with an argument and an example.

For a fractal analysis, it is argued that the average density of the universe is not a primary concept, because no transition to homogeneity needs to be assumed *a priori*, and it is natural to employ the conditional density  $\Gamma(r)$ , namely, the average density at distance  $r$  from an occupied point, or also to employ

$$\Gamma^*(r) = \frac{\int_0^r \Gamma(r') 4\pi r'^2 dr'}{4\pi r^3/3} \quad (4)$$

(Coleman and Pietronero 1992). Given  $\langle \varrho \rangle$ , the conditional density is expressed in terms of the correlation function as

$$\Gamma(r) = \frac{\langle \varrho(\mathbf{r}) \varrho(\mathbf{0}) \rangle}{\langle \varrho \rangle} = \langle \varrho \rangle (\xi(r) + 1). \quad (5)$$

These are the measures employed in several works that find a large scale of homogeneity, e.g., the analyses of the SDSS by Sylos Labini, Vasilyev and Baryshev (2007) and Verevkin, Bukhmastova and Baryshev (2011). In our multifractal analysis of the stellar mass distribution in the SDSS-DR7 (Gaite 2018), the scale of homogeneity is a prerequisite and it is found from the scaling of the second moment of the coarse-grained density in cells of volume  $v$ , namely,

$$\mu_2(v) = \frac{\langle \varrho_v^2 \rangle}{\langle \varrho_v \rangle^2}, \quad (6)$$

which can be expressed as the corresponding average of the correlation function. The power-law fit of  $\mu_2(v)$  by Gaite (2018) is equivalent to a power-law fit of the plain correlation function [and also equivalent to a power-law fit of  $\Gamma(r)$  or  $\Gamma^*(r)$ ]. But one can instead fit the scale-dependent mass variance

$$\mu_2(v) - 1 = \frac{\langle \delta \varrho_v^2 \rangle}{\langle \varrho_v \rangle^2} = \frac{\langle \delta M_v^2 \rangle}{\langle M_v \rangle^2}, \quad (7)$$

which is equivalent to fitting  $\xi(r)$ . Both the two options are displayed in Fig. 1, which we now explain.

Let us look for scaling in a volume limited sample of 1765 galaxies in the redshift range (0.003, 0.013), defined by Gaite (2018) and called VLS1. The solid blue lines in Fig. 1 are the graphs of  $\mu_2$  and  $\mu_2 - 1$ . The fit to the power law

$$\mu_2 = (v/v_0)^{D_2/3-1} \quad (8)$$

in the interval  $v \in [3, 190] \text{Mpc}^3/h^3$  yields  $v_0 = (2000 \pm 180) \text{Mpc}^3/h^3$  and  $\gamma = 3 - D_2 = 1.57 \pm 0.01$ , that is to say,  $D_2 = 1.43 \pm 0.01$  (the power-law fit is a least-squares linear fit of  $\log \mu_2$  versus  $\log v$ ). An analogous fit to the power law

$$\mu_2 - 1 = (v/v_0)^{D_2/3-1} \quad (9)$$

yields  $v_0 = (850 \pm 300) \text{Mpc}^3/h^3$  and  $D_2 = 1.20 \pm 0.06$  ( $\gamma = 1.80 \pm 0.06$ ). Both fits are represented by dashed red lines in Fig. 1. The latter fit, with  $\gamma = 1.80$  and  $v_0^{1/3} = 9.5 \text{Mpc}/h$ , basically agrees with the canonical values of  $\gamma$  and  $r_0$  (from the reduced two-point correlation function of galaxy positions). However, both fits are questionable, because the fractal regime must take place for  $\mu_2 - 1 \approx \mu_2 \gg 1$  and the fitted range extends beyond the small scales where that condition holds. Therefore, some intermediate values

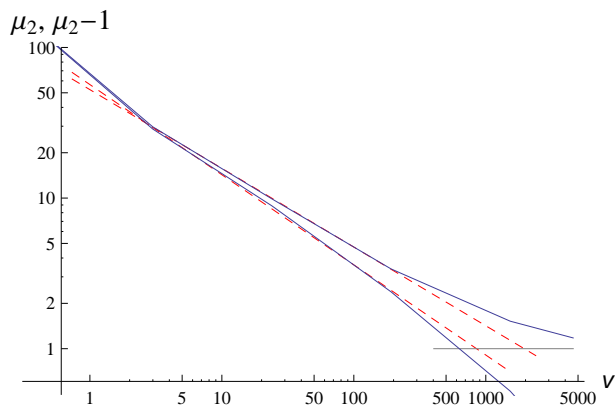


**Fig. 1.** Fits to scaling for sample VLS1: moments  $\mu_2(v)$  and  $\mu_2(v) - 1$  ( $v$  in  $\text{Mpc}^3/h^3$ ), with fits to the scaling  $(v/v_0)^{D_2/3-1}$ , represented as dashed lines. The crossing of each dashed line with the horizontal gray line gives  $v_0$ .

of  $v_0$  and  $\gamma$  should be more appropriate, although these values are difficult to specify, because we have a small range of scales with both  $\mu_2 \gg 1$  and negligible discreteness effects. As is well known, small samples are subject to strong finite size effects (Sylos Labini, Montuori and Pietronero 1998).

To realize the importance of the finite size effects, we can compare them with the statistical errors due to errors in galaxy positions and masses. Gaité (2018) has analyzed how these errors affect the multifractal spectrum of VLS1, with the result that only the right-hand side part of the spectrum is affected (Gaité 2018, left-hand side of Fig. 4). This implies that only the (Rényi) dimensions  $D_q$  with  $q < 0$  are affected. Therefore, the evaluation of  $D_2$  should not be affected. To confirm it, we consider here the uncertainty in the calculation of  $\mu_2(v)$  due to the uncertainty in galaxy positions and masses. For this, we employ the same model as Gaité (2018), namely, we generate ten variant samples, with values of redshift and stellar mass given by, respectively, Gaussian and lognormal distributions with variances in accord with the literature. The variant samples yield ten values of  $\mu_2$  for each value of  $v$ , and we compute for each  $v$  the standard deviation provided by those ten values. The result is that the relative error of  $\mu_2$  is always smaller than 4.2% (the corresponding error bars in Fig. 1 would hardly be visible). The small magnitude of these errors combined with the small magnitude of the errors in the fits shows that the major uncertainty in the fractal analysis is due to the finite size effects, that is to say, to the limitations imposed by the small number of galaxies in the sample and hence the small fractal scaling range.

Gaité (2018) has studied two larger volume limited samples, namely, VLS2, which consists of 16557 galaxies with redshift  $z \in (0.02, 0.03)$ , and VLS3, which consists of 42021 galaxies with  $z \in (0.04, 0.06)$ . Unfortunately,  $\mu_2(v)$  has reduced scaling ranges in these samples and the corresponding power-law fits are quite uncertain. In the case of VLS2, displayed in Fig. 2, the standard error of the slope of the linear fit of  $\log \mu_2$  between 6 and 400  $\text{Mpc}^3/h^3$  is 8.4%. The scaling range of  $\mu_2(v) - 1$  is larger and we can fit it between 6 and 3000  $\text{Mpc}^3/h^3$ , obtaining  $\gamma = 1.56 \pm 0.03$ . However, the fractal regime demands a common scaling of both  $\mu_2$  and  $\mu_2 - 1$ .

Although it could seem that higher- $z$  volume-limited samples should provide larger scaling ranges, we find that

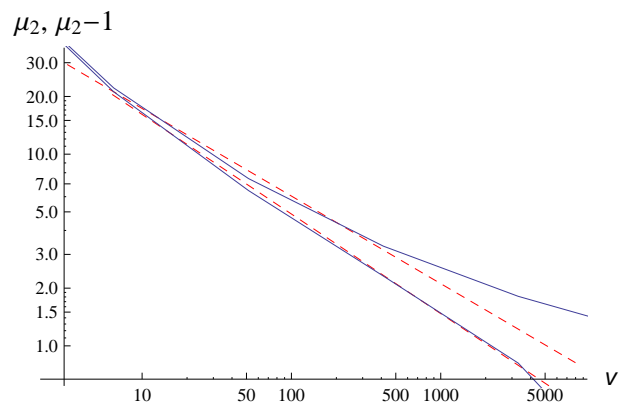


**Fig. 2.** Scaling in VLS2 (following the conventions of Fig. 1). Notice that  $\mu_2(v)$  has a small scaling range.

this is not so. The higher  $z$  is in a volume-limited sample, the more luminous the galaxies in it and the smaller their number density, so that discreteness effects take over growing ranges of the smaller scales, in the fractal regime where  $\mu_2 - 1 \approx \mu_2 \gg 1$ . Notice that the growth of the (absolute value of the) slope of  $\mu_2$  due to discreteness effects occurs in Fig. 2 at a lower value than in Fig. 1. It is to be remarked that this loss of information does not preclude a partial fractal analysis. For example, a relevant part of the multifractal spectrum  $f(\alpha)$  can be calculated from VLS2 and VLS3 (Gaité 2018). On the other hand, in VLS1, the coarse multifractal spectrum for  $v = 1.53 \cdot 10^3$  ( $\text{Mpc}/h$ )<sup>3</sup> is fairly reliable, in spite of  $\mu_2$  being as low as 1.5 (Gaité 2018, Fig. 3). In general, we find that the multifractal spectrum  $f(\alpha)$  is more robust than the spectrum of Rényi dimensions  $D_q$ , although the two functions provide equivalent information from the mathematical standpoint.

In conclusion, the three-dimensional analysis of SDSS-DR7 seems unable to provide precise values of some relevant quantities, in particular,  $D_2$  and  $r_0$ : the most suitable sample, namely, VLS1, only gives the ranges  $D_2 \in (1.2, 1.43)$  and  $v_0^{1/3} \in (8.5, 12.6)$   $\text{Mpc}/h$ . Moreover, this sample only contains low-mass galaxies and cannot be considered representative of the full galaxy population. In general, we should remark that the values of  $D_2$  and  $r_0$  often appear with small relative errors, but these errors correspond to particular fits that do not consider other types of error that are considerably larger, such as the finite size effects that are manifested as uncertainty between the power law fits of  $\mu_2$  and  $\mu_2 - 1$ . Another source of uncertainty in most calculations of  $D_2$  and  $r_0$  is, of course, the absence of galaxy masses.

As an alternative to the study of redshift surveys, it is useful to study angular surveys. In particular, if we discard the redshift and just consider the angular positions in the SDSS-DR7, on the one hand, we do not have to construct volume limited samples, so we have a large number of galaxies available, and, on the other hand, we avoid the redshift space distortions. We study next the properties of fractal angular projections.

### 3. Fractal projections

The study of fractal projections has tradition in mathematics (Falconer 2003; Falconer, Fraser and Jin 2015). In cosmology, the properties of angular projections of fractal sets have been considered in regard to the possibility of a frac-

tal universe with no transition to homogeneity (Mandelbrot 1983; Coleman and Pietronero 1992; Durrer et al. 1997). Of course, the study of the angular projection of the distribution of galaxies, that is to say, of angular galaxy surveys, is old and predates the study of redshift surveys (Totsuji and Kihara 1969; Groth and Peebles 1977). In fact, Peebles (1993) uses the properties of the angular distribution of galaxies as a powerful argument against a fractal universe with no transition to homogeneity. The argument, formulated in terms of just the distribution of galaxy positions, will also be valid here for the stellar mass distribution.

We have to consider, first of all, the generalization of the theory of projection of fractal sets to the theory of projection of fractal *measures*, which has been developed more recently (Falconer, Fraser and Jin 2015). This is necessary because the large-scale mass distribution has to be treated as a measure rather than as a set. In mathematics, a measure on the space  $\mathbb{R}^3$  is a rule that assigns a numerical size to each suitable subset of  $\mathbb{R}^3$ , generalizing the concept of volume (called *Lebesgue measure*). In a mass distribution, the measure is the mass. The *support* of a mass distribution is the smallest *closed set* that contains all the mass. The large-scale mass distribution surely is a multifractal mass distribution of *non-lacunar* type; that is to say, its support is the full space. This property amounts to the absence of *totally empty* cosmic voids. These concepts are explained in detail by Gaite (2019). The non-lacunarity can be observed in the dark matter distribution obtained in cosmological  $N$ -body simulations and is also very likely in the stellar mass distribution (Gaite 2018).

In this regard, let us recall that Durrer et al. (1997) intended to show that the angular projection of a fractal set can have a vanishing lacunarity, with various arguments, mainly, that the projection of a fractal with dimension 2 or higher is non-fractal, but also other arguments related to galaxy properties (apparent sizes and opacities). If the three-dimensional stellar mass distribution is already non-lacunar, then that issue is no longer meaningful. Furthermore, a small lacunarity would also give rise to a non-lacunar projection, because it is certain that the fractal dimension of the support of the distribution is considerably larger than two (Gaite 2018).

The study of projections of multifractal mass distributions is not reduced to the behaviour of lacunarity. If we characterize a mass distribution by its dimension spectrum  $D_q$ , the question of how this spectrum behaves under projections has been partially answered by Hunt and Kaloshin (1997). The answer is the natural generalization of the standard result for fractal sets (Falconer 2003; Falconer, Fraser and Jin 2015): in particular, the dimension of the projection of a fractal set onto a plane (or a smooth surface) equals the dimension of the set if it is smaller than two and it is two otherwise (this statement has to be qualified for non-random fractals, which can have special projections along some directions). This result is still valid for the dimension spectrum  $D_q$  of a mass distribution, with the restriction that  $1 < q \leq 2$  (Hunt and Kaloshin 1997). The restriction is due to technical reasons and may not apply to some types of mass distributions, but we are mostly interested in that interval and, especially, in the correlation dimension  $D_2$ . Since we expect that  $D_2$  is in the range 1.2–1.4 for the stellar mass distribution (Sect. 2), it has to be preserved under angular projections.

Here, we should notice that some authors find that  $D_2 \geq 2$  (Jones et al. 2004, table 1). However, large values of  $D_2$  often come from power-law fits of  $\xi(r) + 1$  [or  $\Gamma(r)$ ,  $\Gamma^*(r)$ ], on scale ranges that extend too far and include a quasi-homogeneous range, thus being biased towards  $D_2 = 3$ , as explained in Sect. 2. Moreover, all those values of  $D_2$  refer to the galaxy number density.

The dimension spectrum  $D_q$  of a mass distribution can be calculated from the scaling of the fractional statistical moments (Harte 2001). The standard type of fractional statistical moment employed in multifractal analysis,  $\mathcal{M}_q$ , can be calculated by coarse-graining the mass distribution with a partition in cells of linear size  $l$ . The coarse-graining statistical moment is

$$\mathcal{M}_q(l) = \sum_i \left( \frac{m_i}{M} \right)^q, \quad (10)$$

where the index  $i$  runs over the set of non-empty cells,  $m_i$  is the mass in the cell  $i$ , and  $M = \sum_i m_i$  is the total mass. Then, multifractal behavior is given, for  $l \rightarrow 0$ , by

$$\mathcal{M}_q(l) \sim l^{\tau_q}, \quad (11)$$

and the dimension spectrum is given by

$$D_q = \frac{\tau_q}{q-1} \quad (12)$$

(in particular,  $D_2 = \tau_2$ ). In an angular projection partitioned in cells of solid angle  $\Omega$ , the length  $l$  is to be replaced by  $\Omega^{1/2}$ .

The correlation dimension  $D_2$  can also be measured in angular catalogs of galaxies by calculating the angular two-point correlation function. The angular two-point correlation function of galaxies is defined in analogy with its three-dimensional counterpart and can be calculated from it (Totsuji and Kihara 1969; Groth and Peebles 1977; Peebles 1993). However, the usual definition of correlation functions of galaxies refers to their positions and we are interested in correlations of the stellar mass distribution; so we have to employ mass density instead of number density, for example, in Eq. (3). The second moment of the coarse-grained angular mass density in cells,  $\mu_2$ , can be obtained as the average of the correlation function of the mass density and it is simply related to  $\mathcal{M}_2$  as

$$\mu_2(\Omega) = \frac{\langle \varrho_\Omega^2 \rangle}{\langle \varrho_\Omega \rangle^2} = \frac{\mathcal{M}_2(\Omega)}{\Omega} \quad (13)$$

(assuming that  $\Omega$  is normalized to the total solid angle). This formula is a particular case of the formula that gives the relationship between  $\mathcal{M}_q$  and the coarse-grained mass density  $q$ -moment (see, e.g., Gaite 2019). For a spherical mass distribution this relationship can be written as

$$\mu_q(\Omega) = \frac{\langle \varrho_\Omega^q \rangle}{\langle \varrho_\Omega \rangle^q} = \frac{\mathcal{M}_q(\Omega)}{\Omega^{q-1}} \quad (14)$$

(it is assumed that  $q > 0$ ). Therefore, the expected scaling exponent for  $\mu_q(\Omega)$  is

$$\tau_q/2 - (q-1) = (q-1)(D_q/2 - 1). \quad (15)$$

In particular,  $\mu_2(\Omega)$  is expected to scale with exponent  $D_2/2 - 1$ . Naturally, the exponent  $(q-1)(D_q/2 - 1)$  is

only valid provided that  $D_q < 2$ , because 2 is the maximal fractal dimension of a two-dimensional projection, in accord with the results of Hunt and Kaloshin (1997).

To proceed, let us recall and generalize some standard results about the two-point correlation of angular positions, in the light of the theory of fractal projections.

#### 4. The angular correlation of galaxies

The reduced two-point correlation function of the angular positions in a magnitude-limited sample, denoted  $w(\theta_{12})$ , can be expressed as an integral of the two-point correlation function of ordinary positions  $\xi(r_{12})$  over the radial coordinates  $r_1$  and  $r_2$ . The integral can be simplified if  $\xi(r)$  follows a power-law, Eq. (1). Then, in the small-angle approximation,  $\theta \ll 1$  (in radians), the integral gives

$$w(\theta) = K \theta^{1-\gamma} \left( \frac{r_0}{d_*} \right)^\gamma \int_{-\infty}^{\infty} \frac{dx}{(1+x^2)^{\gamma/2}}, \quad (16)$$

where  $K$  is a nondimensional constant that depends on  $\gamma$  and the radial selection function, and  $d_*$  is the characteristic sample depth (Peebles 1993). The integration variable is  $x = (r_2 - r_1)/(r_1\theta)$ . The integral over  $x$  is left unevaluated to show that the present approximation fails if the integral is divergent, namely, if  $\gamma \leq 1$ . In this case, the projected correlation function is dominated by pairs of points at large relative radial distances.

Although the definition of  $w(\theta)$  and Eq. (16) are commonly assumed to refer to galaxy positions, they are equally applicable to the stellar mass distribution or any mass distribution. In the strong clustering regime,  $D_2 = 3 - \gamma$ , so the cases  $\gamma > 1$  or  $\gamma \leq 1$  correspond, respectively, to  $D_2 < 2$  or  $D_2 \geq 2$ , the latter being the case of non-fractal projection. If  $\gamma > 1$ , then the projected correlation function is dominated by pairs of points at small relative radial distances, so the three-dimensional fractal structure, as a set of short-distance geometric properties, is preserved in the projection.

It is also useful to notice that  $K$  and the integral in Eq. (16), for  $\gamma > 1$  and not too close to one, are factors of the order of unity, so the magnitude of  $w(\theta)$  is ruled by the quotient  $r_0/d_*$  (Peebles 1993). If the characteristic sample depth is much larger than  $r_0$ , as is normal in deep surveys, the angular correlations are small, except at very small angles. This means that the projected fractal structure, which requires large fluctuations, that is to say,  $w(\theta) \gg 1$ , is only observable at very small  $\theta$ . In contrast, the exponent  $\gamma$  can possibly be measured in a larger range of values of  $\theta$ , provided that the power law form of Eq. (16) holds in that range. However, a value of  $\gamma$  measured *only* in a range of  $\theta$  that corresponds to a quasi-homogeneous distribution may not give information of fractal properties. In contrast, if  $w(\theta) \propto \theta^{1-\gamma}$  and is large for very small  $\theta$ , then  $w(\theta) \propto \theta^{D_2-2}$ , because  $\gamma = 3 - D_2$ . Furthermore, the average of  $w(\theta)$  over a small cell of solid angle  $\Omega$  is large and proportional to  $\Omega^{D_2/2-1}$ . Therefore,

$$\mu_2(\Omega) \approx \mu_2(\Omega) - 1 \sim \Omega^{D_2/2-1},$$

as already seen in Sect. 3.

However, it is obvious that the cosmic fractal structure appears blurred in angular images of the galaxy distribution, that is to say, the cosmic web features are hardly perceptible, as is illustrated, for example, by the image of the

Lick survey (Peebles 1993, Fig. 3.9). These images are proof of large scale homogeneity, namely, of a small ratio  $r_0/d_*$ , but do not reveal the cosmic web features that are so conspicuous in slices of three dimensional redshift surveys. If the cosmic web were an ideal mathematical fractal distribution, its features would appear in the projection at very small angles, that is to say, zooming in on an angular image of the mass distribution. But the galaxies have discrete nature. In this respect, we should notice that  $x$  is integrated down to zero in Eq. (16), whereas correlation functions are actually calculated as sums over pairs of points in a finite set. In particular, there is a minimal distance for some pair, while the density of projected far points on the angular location of that pair keeps growing as  $d_*$  grows. It is evident that uncorrelated far points must blur the small scale features and even obliterate them at some stage.

The cosmic web structure also fades in the three-dimensional mass distribution when its sampling by galaxies does not have a sufficiently high number density to probe scaling well below  $r_0$ , where  $\xi$  is large. We have already noticed this problem in Sect. 2, as regards our volume limited samples from SDSS-DR7. Of course, one can also analyze scales where  $\xi < 1$ , namely, the scales of the transition to homogeneity, and perhaps find that the power law of Eq. (1) provides a good fit in some range of scales. This power law, however, will not be necessarily related to the strong clustering, fractal regime, and it will just show the presence of a type of weak clustering regime called *critical regime* by Gaite, Domínguez and Pérez-Mercader (1999), in analogy with the theory of critical phenomena in condensed matter physics.

It can be concluded from the preceding arguments that the analysis of angular catalogs can be deceptive, as regards the strong clustering regime. To see this most simply, let us consider a three-dimensional mass distribution that may be strongly clustered and that is randomly sampled by equivalent points with a given mean number density. If this number density is so low that the sample does not show strong clustering at all, then its angular projection cannot show strong clustering either, in spite of the fact that the mean angular number density grows without limit with the depth of the three-dimensional sample. Therefore, very deep angular galaxy catalogs may not be probing the strong clustering regime. The criterion to ensure that an angular catalog is probing the strong clustering regime is, of course, that the range of scales where  $w(\theta) \gg 1$  must not be dominated by discreteness effects. In particular, if a non-trivial power law fit has been obtained in a range of scales, this range must include a subrange of the smaller scales where  $w \gg 1$ . Let us examine if the calculations of the two-point correlation function of angular positions of galaxies fulfill this criterion and to what extent.

Peebles (1993, Fig. 7.2) shows log-log plots of  $w(\theta)$  for the Zwicky, Lick and Jagellonian catalogs. As noticed above, the image of the Lick survey looks quasi-homogeneous rather than fractal. In fact, only the Zwicky catalog, with limiting apparent magnitude  $m = 15$ , has a range of small  $\theta$  with  $w(\theta) > 1$ . However, the absolute value of the slope grows in that range, probably tending to two, the value that corresponds to  $\gamma = 3$  and  $D_2 = 0$ , that is to say, to a distribution of *isolated* points. Something similar happens in the plot of  $w(\theta)$  for successive slices of the APM catalog with  $\Delta m = 0.5$  (Peebles 1993, Fig. 7.3). Analyses of modern and hence deeper catalogs

seldom show any  $w > 1$ . For example, the analysis of the SDSS-DR7 angular two-point correlation function by Wang, Brunner and Dolence (2013) has a very small range of  $\theta$  with  $w(\theta) > 1$  and only for the apparent-magnitude slice  $17 < r \leq 18$  (Wang, Brunner and Dolence 2013, Fig. 15). Among all the cited calculations of  $w(\theta)$ , only the one for the Zwicky catalog allows us to speak of the strong clustering regime, although the range with  $w > 1$  does not allow to fit a power law and, moreover, already shows discreteness effects. Wang, Brunner and Dolence start at apparent magnitude  $r > 17$ , but there is a large number of galaxies of lower magnitude in the SDSS-DR7 that we can use.

In conclusion, the available calculations of  $\gamma$  from the the scaling of the angular correlation function  $w(\theta)$  are confined to quasi-homogeneous projections and are hardly suitable to obtain fractal properties (such as fractal dimensions). Nevertheless, the study of  $w(\theta)$  in a quasi-homogeneous projection is suitable to calculate the homogeneity scale  $r_0$ . We shall confirm these conclusions in the following.

### 5. Angular analysis of the stellar mass distribution

We employ the same SDSS-DR7 data from the NYU-VAGC employed by Gaité (2018), and we also select the apparent magnitude range  $12.5 < m_r < 17.77$ . The angular ranges are defined in terms of equal-area coordinates  $sl = \sin \lambda$  and  $f = \eta + 0.567$  radians, where the angles  $\lambda$  and  $\eta$  constitute the SDSS coordinate system (the details of the definition of  $sl$  and  $f$  are given by Gaité 2018). The available ranges of our coordinates are  $-0.760 < sl < 0.793$  and  $-0.0227 < f < 1.200$  (radians), providing a total solid angle  $\Omega = 1.554 \cdot 1.222 = 1.899$  steradians that contains 529 967 galaxies.

In the angular rectangle so defined, we use coarse multifractal analysis, with the same lattice of cells as in Gaité (2018), but without dividing the radial coordinate; that is to say, we use a  $4 \times 3$  basic lattice and a sequence of binary subdivisions. The corresponding cells have an aspect ratio close to one, which is convenient. Given that the size of the cells of the basic lattice is somewhat small to appreciate the behaviour at large angles, we add two coarser lattices, namely, a  $3 \times 2$  lattice and a  $2 \times 2$  lattice.

The goal of multifractal analysis is to obtain either the dimension spectrum  $D_q$  or the multifractal spectrum  $f(\alpha)$ . For the angular distribution of stellar mass, as a projected mass distribution, we know that  $D_q$  is preserved from the three-dimensional distribution in the interval  $1 < q \leq 2$ , as long as  $D_q < 2$  (Sect. 3). In general,  $D_q$  is a non-increasing function of  $q$ . From redshift-space calculations, we have that  $D_2$  is in the range 1.2–1.4 (Sect. 2) and that  $D_q$ , for diminishing  $q$ , reaches 2 for some  $q > 1$  and is definitely larger than 2 for  $q = 1$ , namely,  $D_1 \simeq 2.4$  (Gaité 2018). Since there is only a small subinterval  $[q, 2]$  in which  $D_q < 2$ , the correlation dimension  $D_2$  is representative of the projected stellar mass distribution. This dimension can be obtained from a power-law fit of either the angular two-point correlation function or the coarse-grained density variance.

We first analyze the full set of 529 967 galaxies (a magnitude-limited sample) to calculate the coarse-grained density statistical moment

$$\mu_2(\Omega) = \frac{\langle \varrho_\Omega^2 \rangle}{\langle \varrho_\Omega \rangle^2} = \frac{\langle M_\Omega^2 \rangle}{\langle M_\Omega \rangle^2}, \quad (17)$$

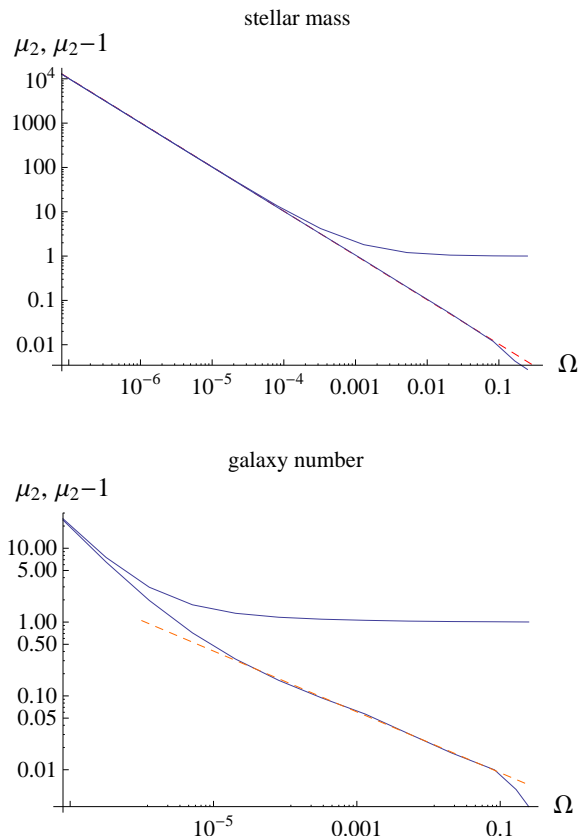


**Fig. 3.** Second moment  $\mu_2(\Omega)$  and variance  $\mu_2(\Omega) - 1$  for the stellar mass (above) and number distributions (below), with linear fits (dashed lines) in a range of  $\Omega$  ( $\Omega$  normalized). They give  $\gamma = 3$  and  $\gamma = 1.82$ , respectively.

where  $\Omega$  is the cell solid angle (the angular area) and  $M_\Omega$  is the cell mass. According to Eq. (16), the expected scaling of the variance is

$$\mu_2(\Omega) - 1 = \frac{\langle \delta M_\Omega^2 \rangle}{\langle M_\Omega \rangle^2} = \left( \frac{\Omega}{\Omega_0} \right)^{-(\gamma-1)/2}, \quad (18)$$

where  $\Omega_0$  is the solid angle at which the projected distribution approaches homogeneity and can be expressed in terms of  $K$ ,  $r_0/d_*$  and  $\gamma$ . We calculate  $\mu_2(\Omega)$  taking into account the stellar masses of the galaxies and also suppressing them. The latter calculation is equivalent to the calculation of the two-point correlation function of galaxy angular positions. In these calculations, we could consider the uncertainty in galaxy positions and masses, like in Sect. 2. However, the consequent errors are even more negligible than in Sect. 2, due to the averaging effect of the projection. At any rate, there are larger uncertainties, like in the analysis of volume limited samples in Sect. 2.

#### 5.1. Full magnitude-limited sample

In Fig. 3 are the log-log plots of  $\mu_2(\Omega)$  and  $\mu_2(\Omega) - 1$  for the stellar mass and galaxy number distributions ( $\Omega$  is normalized to the total solid angle from now onwards, unless the contrary is stated). Evidently, the effect of considering the stellar mass is very significant. The power-law fits of  $\mu_2(\Omega) - 1$  in the range  $\Omega \in [2 \cdot 10^{-5}, 8.3 \cdot 10^{-2}]$  (as linear log-log fits) yield  $(\gamma - 1)/2 = 1.000 \pm 0.004$  for the stellar

mass and  $(\gamma - 1)/2 = 0.412 \pm 0.005$  for the galaxy number. The first fit can be extended to a very large range of scales, which also includes a large range with  $\mu_2 \gg 1$ . But this is hardly useful, because the exponent  $\gamma = 3$  corresponds to  $D_2 = 0$ , that is to say, the dimension of a set of isolated point-like masses, as if the small-scale discreteness held over the full range of scales. The second fit holds in a smaller but substantial range and gives  $\gamma = 1.82$ , compatible with the results of Wang, Brunner and Dolence (2013). However, the range with  $\mu_2 \gg 1$ , where  $\mu_2$  and  $\mu_2 - 1$  tend to coincide and which could be the fractal range, also corresponds to  $D_2 \rightarrow 0$ : indeed, the power-law fit of  $\mu_2(\Omega) - 1$  in  $\Omega \in [8 \cdot 10^{-8}, 1.3 \cdot 10^{-6}]$  gives  $(\gamma - 1)/2 = 0.90 \pm 0.02$ . In contrast, the value of  $\mu_2 - 1$  is well below one in the range where  $\gamma = 1.82$ , that is to say, this range corresponds to a quasi-homogeneous distribution. Since the transition to homogeneity is defined by  $\mu_2(\Omega_0) - 1 = 1$ , from Eq. (18), the comparison between the upper and lower plots shows that it takes place at very different scales. For example, at  $\Omega = 10^{-5}$ , the stellar mass has  $\mu_2 - 1 = (\delta M/M)^2 \gg 1$ , but  $\delta N/N$  is small.

The effect of the galaxy stellar masses is so important because of the distribution of these masses along the radial coordinate. To realize this, let us compare how galaxy number counts and stellar mass are distributed with respect to redshift. Both quantities are roughly distributed in a similar way; namely, there are few galaxies and little stellar mass at low redshift, but both quantities grow to reach their maxima at some intermediate redshift and then decrease again. This behaviour is a consequence of the geometry of the survey and the apparent-magnitude cut, which are such that the available volume grows with  $z$  while the number density of visible galaxies diminishes. However, while the volume growth is indifferent to the stellar masses, the apparent-magnitude cut is not, because the galaxies that can be observed at high  $z$  are necessarily very luminous and hence very massive. Therefore, the stellar mass reaches its maximum at a higher  $z$  and the mean mass per galaxy strongly grows at high  $z$ . The difference in the distributions of galaxy numbers and masses of our sample is shown in Fig. 4.

Now we can understand why we have found the value  $D_2 = 0$  that corresponds to a set of isolated point-like masses: it is due to the very massive galaxies in the sample, most of which are placed at high redshift and are practically isolated in the sample (although not in reality). Because of their small number, they have a negligible effect on the moments of the galaxy number distribution, but they can have, because of their masses, an overwhelming effect on the statistical moments of the stellar mass distribution. Of course, it is possible to reduce the apparent-magnitude cut and so remove many high- $z$  galaxies, but this simple recipe will not work: the problem lies in the construction of these apparent-magnitude samples, because some very massive galaxies at high  $z$  have low apparent magnitudes. Indeed, we have tried cuts at  $m_r < 16$  (keeping 53237 galaxies) and at  $m_r < 15$  (keeping 13156 galaxies), and the  $D_2 = 0$  distribution along the full range of scales persists.

However, the fractal analysis of volume-limited samples in Sect. 2 basically agrees with the corresponding analyses without galaxy masses in the literature, and moreover they all basically agree with the value of  $\gamma$  in the angular analysis without galaxy masses. Therefore, we expect that a suitable modification of the full magnitude-limited sample that removes the isolated and very massive galaxies can make the

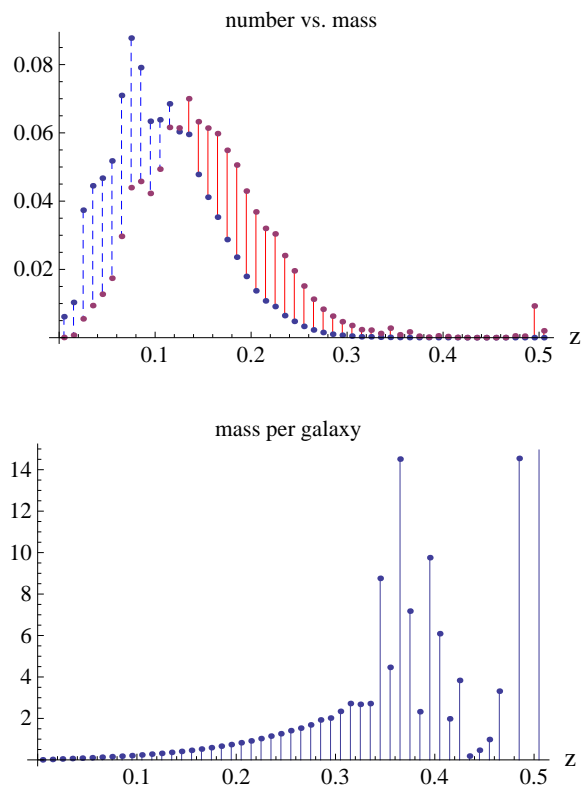


**Fig. 4.** (Above) Galaxy number fraction versus stellar mass fraction in redshift bins  $\Delta z = 0.01$ . Blue dashed and red solid segments denote number and mass dominance, respectively. (Below) Mean mass per galaxy in the same bins, in multiples of  $10^{11} M_{\odot}$ .

angular analysis with galaxy masses agree as well. We find two ways of suppressing the effect of the offending galaxies. First, we can take advantage of having the galaxy redshifts available. A natural way to segregate the isolated and very massive galaxies is to put a redshift cutoff (Sect. 5.2). Second, we can directly deal with the effect of isolated and very massive galaxies as a shot noise effect that must be suppressed before computing  $\mu_2(\Omega) - 1$ . We know that the shot noise or discreteness error is always important at very small scales and we have indeed seen that  $D_2 \rightarrow 0$  when its effect is dominant. It is not necessary to suppress the shot noise when it only appears for very small coarse-graining lengths, but it seems that the shot noise is important at all scales in the calculation of the angular mass variance, so we need to suppress it (Sect. 5.3).

## 5.2. Samples with redshift cutoffs

The decreasing galaxy number density with distance (or redshift) in an apparent-magnitude limited sample is normally accounted for by the *selection function*, which represents the probability that a galaxy at a given distance is included in the sample. While this function is sufficient for galaxy number counts, it does not discriminate galaxies by their masses and, therefore, is not sufficient in our case. A more sophisticated procedure could take masses into account and correct the variable galaxy mass range with redshift, but we can use a simpler method.

A redshift cutoff effectively removes massive galaxies with low number density, as can be deduced from Fig. 4.

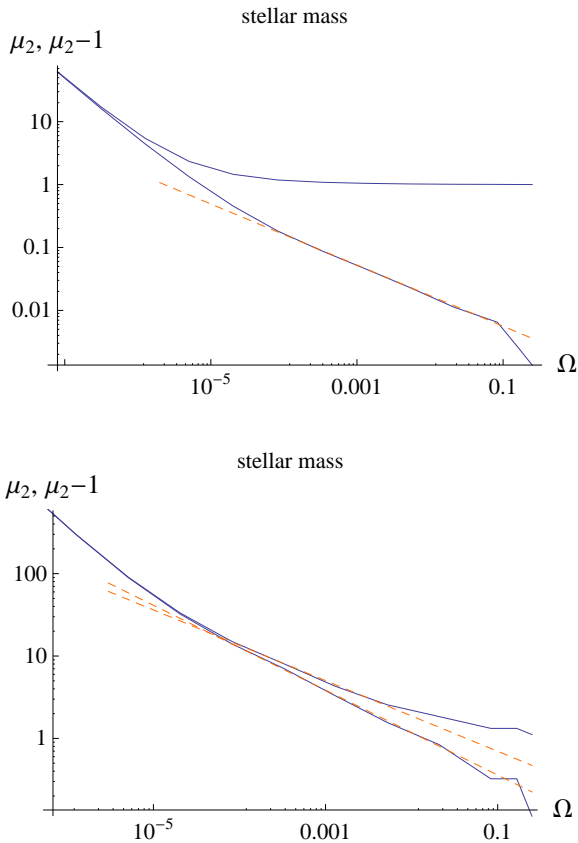


**Fig. 5.** Second moment  $\mu_2$  and variance  $\mu_2 - 1$  for the projected stellar mass of two samples with redshift cutoffs: (above) cut-off at redshift  $z = 0.34$ , with a power-law fit giving  $\gamma = 1.97$ ; (below) cutoff at redshift  $z = 0.025$ , with a power-law fit giving  $\gamma = 1.83$ , for  $\mu_2$ , and  $\gamma = 2.03$ , for  $\mu_2 - 1$ .

The lower plot suggests us to cut at  $z = 0.34$ , although the appearance of the plot somewhat depends on the magnitude of the redshift bin. At any rate, the cut at  $z = 0.34$  is suitable because it removes from the full sample only 245 galaxies, which amount to a 6.5% of mass, but has a drastic effect on the values of  $\mu_2$  and  $\mu_2 - 1$  for the stellar mass distribution: as can be seen in Fig. 5, upper plot, now the graphs of  $\mu_2$  and  $\mu_2 - 1$  for the stellar mass distribution look like the ones for the galaxy number distribution in Fig. 3. However, the exponent of the power-law fit of  $\mu_2(\Omega) - 1$  (in  $\Omega \in [8 \cdot 10^{-5}, 8 \cdot 10^{-2}]$ ) is somewhat larger in absolute value, namely,  $(\gamma - 1)/2 = 0.486 \pm 0.008$ , giving  $\gamma = 1.97 \pm 0.02$ . Again, in the range of this fit,  $\mu_2 - 1 \ll 1$ , while we find that  $\gamma$  tends to three in the range of  $\Omega$  where  $\mu_2 - 1 \gg 1$ , due to the inevitable discreteness at very small  $\Omega$ . Therefore, this projected stellar mass distribution is quasi-homogeneous, with small fluctuations that are power-law correlated (see the appearance of this projected mass distribution in the upper image of Fig. 6).

The projected stellar mass distribution is quasi-homogeneous because it is a deep projection and the cosmic web features are obliterated in the projection, as explained in Sect. 4. Of course, we can have shallower projections by setting lower redshift cutoffs. To choose an appropriate value of  $z$ , we can appeal to a heuristic argument: if we want to preserve the cosmic web features, we should not go too deep into the homogeneous regime. As said in Sect. 4, the criterion for a sample of equal-mass particles

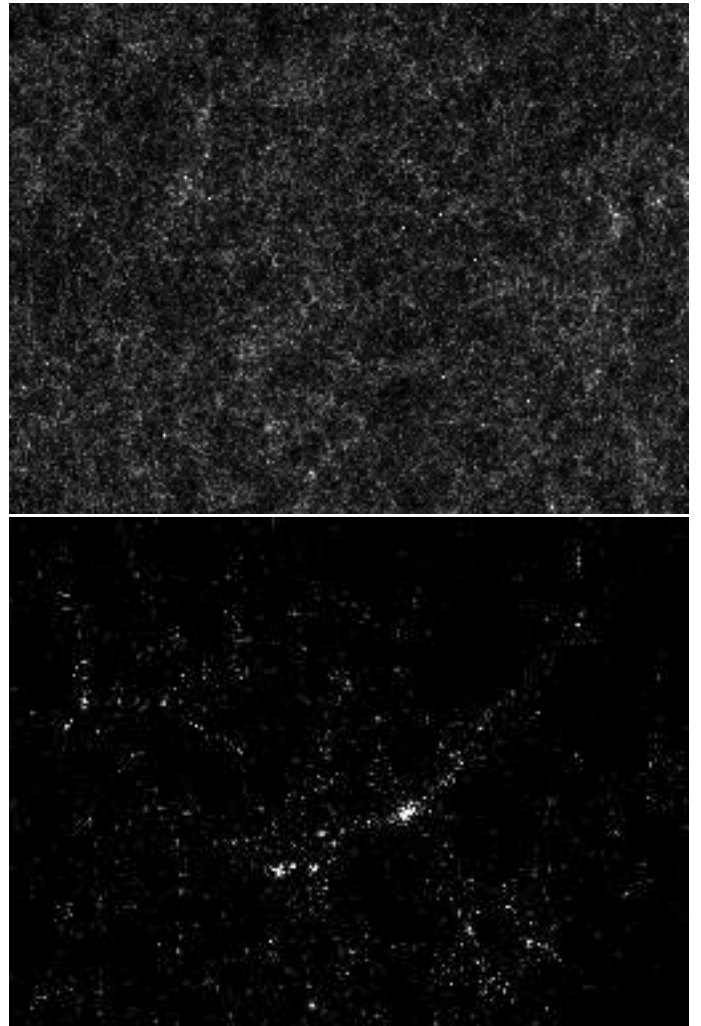


**Fig. 6.** Projected stellar mass distributions for the two samples with redshift cutoffs: (above) quasi-homogeneous distribution for the  $z = 0.34$  cut; (below) cosmic web for the  $z = 0.025$  cut.

is that the mean distance between projected uncorrelated points is larger than the minimal distance between correlated points. However, it is hard to translate this qualitative criterion into a quantitative one, especially, for unequal masses. According to Sect. 2, we can take  $30 h^{-1} \text{Mpc}$  as a safe scale for homogeneity, so we can try some small multiple of  $z = 0.01$ , e.g.,  $z = 0.025$ . The corresponding sample contains 18168 galaxies.

For this sample,  $\mu_2$  and  $\mu_2 - 1$  are plotted in Fig. 5, lower part, and show a notable improvement. Indeed, the projected mass distribution is not quasi-homogeneous in this case, because the power law holds in a range with  $\mu_2 - 1$  up to 10, that is to say, in the (moderately) strong clustering regime. Moreover, the features of the cosmic web structure are obvious in the mass distribution that is represented in the lower image of Fig. 6. The power-law fit of  $\mu_2 - 1$  gives  $\gamma = 2.03 \pm 0.02$  (in  $\Omega \in [8 \cdot 10^{-5}, 2 \cdot 10^{-2}]$ ), almost the same as with the cutoff  $z = 0.34$  ( $\gamma$  is actually a bit larger, so it further departs from the value given by the galaxy number). Because this value holds for strong clustering, we can interpret that it gives the correlation dimension  $D_2 = 3 - \gamma \simeq 1$ , which is smaller than expected. But we have to

notice, like in Sect. 2, that it is necessary to consider, in the fractal regime, the convergence of the respective fits of  $\mu_2 - 1$  and  $\mu_2$ . Although  $\mu_2$  has a smaller scaling range, the fit in  $\Omega \in [8 \cdot 10^{-5}, 5 \cdot 10^{-3}]$  gives  $\gamma = 1.83 \pm 0.02$  and, hence,  $D_2 = 1.17 \pm 0.02$ , with small relative error. The resulting range  $D_2 \in (1, 1.2)$  is to be compared with the range  $D_2 \in (1.2, 1.4)$  obtained from the analysis of volume-limited samples in Sect. 2. It is not clear which type of analysis is preferable and, unfortunately, the ranges of  $D_2$  do not overlap.

Apart from the correlation dimension, we are interested, of course, in the scale of transition to homogeneity, which can be found by first solving the equation  $\mu_2(\Omega_0) - 1 = 1$ , then solving for  $r_0/d_*$  as a function of  $\Omega_0$ ,  $K$  and  $\gamma$ , and last estimating  $d_*$ . Before we do this, let us consider the important issue of discreteness effects.

### 5.3. Shot noise suppression

As is well known, the Poissonian fluctuations of an uncorrelated distribution of points in some volume are characterized by a number density variance equal to  $1/N$ , where  $N$  is the mean number of points. This term is also present when the points are correlated. In the case of a distribution of particles (massive points), such as the galaxy distribution, and assuming that the masses are statistically independent of the positions, the shot noise term becomes

$$\frac{\langle m^2 \rangle}{\langle m \rangle^2 N}$$

(Peebles 1993, pg. 509–510).

For a sample of  $N$  particles, the calculation of the moment  $\mathcal{M}_2$  by Eq. (10), when the cell size is so small that no cell contains more than one particle and therefore the sums over cells and over particles coincide, obtains the shot noise term

$$\frac{\sum m_i^2}{(\sum m_i)^2} = \frac{\langle m^2 \rangle}{\langle m \rangle^2 N}, \quad (19)$$

where the index  $i$  of the sums runs over the set of particles.

If we start with a cell size such that no cell contains more than one particle and let the cell size grow, then, at some point, some cells contain more than one particle and the sum over those cells in Eq. (10) is larger than the sum over the particles in the cells. Therefore, the term (19) is the minimum value of  $\mathcal{M}_2$ , and while  $\mathcal{M}_2$  stays constant,  $D_2 = 0$ , according to Eqs. (11) and (12). At some scale,  $\mathcal{M}_2$  starts growing and the correlation terms, coming from cells with several particles, become larger than the shot noise term, so there is a crossover to the scaling with the corresponding dimension  $D_2 > 0$ .

For a given set of particles, the factor  $\langle m^2 \rangle / \langle m \rangle^2$  in Eq. (19) is their normalized mass variance plus one and its magnitude is independent of the correlations between the particle positions. The factor takes its minimal value, equal to one, for equal masses, and it is close to one for a Gaussian distribution of masses, with a small variance.

Peebles (1993) says about the shot noise term: “In most applications to be discussed here, this shot noise term is subdominant and will be dropped.” This indeed happens in our calculation of  $\mu_2(\Omega) - 1$  with equal masses, because the shot noise term (19) reduces to  $1/N = 1/529967$ , which is very small and is indeed subdominant except at very

small values of  $\Omega$ , as we shall see below. However, the distribution of galaxy masses in our sample is *very* far from being Gaussian and actually  $\langle m^2 \rangle / \langle m \rangle^2 = 538$ . Naturally, this very large value is due to the presence of very massive galaxies, in a small number but that is much larger than it would be in a volume-limited sample. The removal of high- $z$  massive galaxies, namely, of galaxies with  $z > 0.34$ , as in Sect. 5.2, severely reduces the galaxy mass variance, yielding  $\langle m^2 \rangle / \langle m \rangle^2 = 2.54$ , which still corresponds to a strongly non-Gaussian mass distribution and gives a non-negligible shot noise term. Peebles (1993) advises that, where the shot noise term is appreciable, it is to be subtracted.

The suppression of shot noise always eliminates the effect that isolated massive galaxies have on  $\delta M_\Omega / M_\Omega$ , so that the subtracted magnitude no longer has a scaling that corresponds to the exponent  $\gamma = 3$ . However, the primitive value of the normalized galaxy mass variance, namely, 538, is too large and causes several problems. Indeed, it results in a shot noise term (19) that is dominant in  $\mathcal{M}_2(\Omega)$  up to the value  $\Omega \simeq 10^{-3}$ . At this value,  $\mu_2(\Omega) - 1 \simeq 1$ , that is to say, the mass density is quasi-homogeneous, as can be seen in the upper plot of Fig. 3. Moreover, we find that  $\mu_2(\Omega) - 1$  becomes negative for  $\Omega \geq 2.1 \cdot 10^{-2}$ . This may seem surprising, but the subtraction from  $\mathcal{M}_2(\Omega)$  changes  $\mu_2(\Omega)$  as well, in accord with Eq. (13), so  $\mu_2(\Omega) - 1$  is no longer the normalized variance of the mass  $M_\Omega$  (although we keep the same notation). The variance is forced to be positive but the subtracted value is not. A consequence of  $\mu_2(\Omega) - 1$  becoming negative for  $\Omega \geq 2.1 \cdot 10^{-2}$  is that the available scaling range is significantly smaller and, in fact, there is no good scaling.

Therefore, it is right to remove the  $z > 0.34$  galaxies and work with the more sensible value of the normalized galaxy mass variance  $\langle m^2 \rangle / \langle m \rangle^2 = 2.54$ . Let us see the effect of subtracting the shot noise term (19) from  $\mathcal{M}_2(\Omega)$  in both the cases with and without mass information. In the case in which the masses are taken equal, the power-law fit of  $\mu_2(\Omega) - 1$  in the range  $\Omega \in [2 \cdot 10^{-5}, 8.3 \cdot 10^{-2}]$  yields  $(\gamma - 1)/2 = 0.376 \pm 0.009$ , and hence  $\gamma = 1.75$ , which is close to the value obtained in Sect. 5.1, and in fact agrees better with the result of Wang, Brunner and Dolence (2013). In the case with the stellar masses, the subtraction of the shot noise term has the effect that the plot of  $\mu_2(\Omega) - 1$  approaches the plot for equal masses and actually shows a better scaling for small  $\Omega$ . Indeed, it is possible to make a power-law fit in the range  $\Omega \in [1.3 \cdot 10^{-6}, 8.3 \cdot 10^{-2}]$ , which yields  $(\gamma - 1)/2 = 0.415 \pm 0.007$  (with a small error in a long scaling range). This fit gives  $\gamma = 1.83$ , which is close to but a little larger than the value for equal masses. It agrees well with the result of Li and White (2009), whose procedure automatically suppresses the shot noise.

As a general remark, we must notice the different conceptual nature of the shot noise in a galaxy-galaxy correlation analysis and in a multifractal analysis. In the former, galaxies are considered as equivalent point-like particles, like molecules in a gas. In the latter, galaxies are just mass concentrations that may not be point like. Actually, the standard multifractal analysis of mass distributions assumes that the mass concentrations are power-law density singularities and are located *densely*, that is to say, they can be found inside any ball, however small (see, e.g., Gaite 2019). Therefore, the description of the stellar mass distribution as a set of *separated* galaxies with definite locations and masses is actually a sort of coarse-grained description

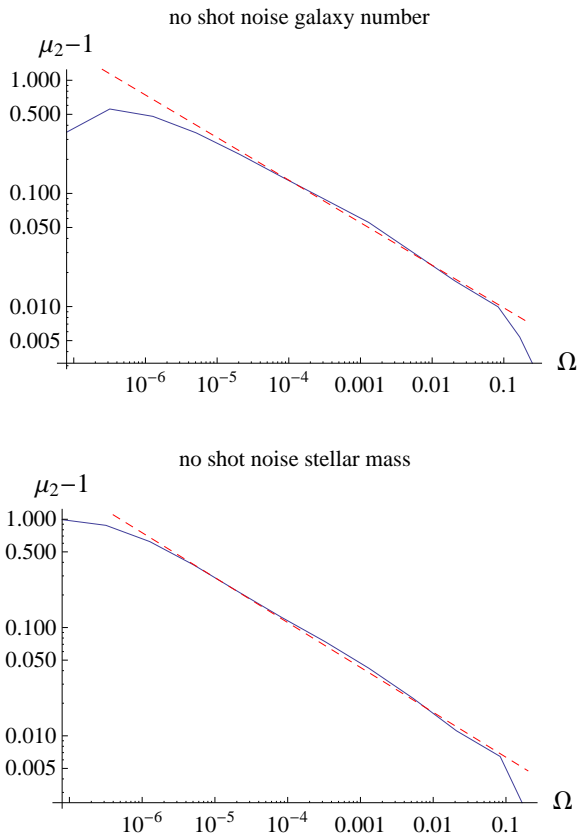


**Fig. 7.** Values of  $\mu_2(\Omega) - 1$  after shot noise suppression, for the distributions of galaxy number (above) and stellar mass (below), with linear fits (dashed lines). They give  $\gamma = 1.75$  and  $\gamma = 1.83$ , respectively.

that only holds at certain spatial resolutions, namely, for coarse-graining lengths larger than a prescribed galaxy size. This size may not be arbitrary when all the relevant physics is taken into account, but it is surely arbitrary in the context of the large scale structure of the universe in the LCDM model, given the absence of scales in the gravitational dynamics.

At any rate, we could define as particles entities larger than galaxies, such as clusters of galaxies. Of course, in the cell-based multifractal analysis, there is a minimum cell size, at which  $\mathcal{M}_2$  becomes constant, imposed by the nature of the galaxy data; and the subtraction of that constant is supposed to remove the “shot noise”. However, the mass concentrations that correspond to a larger cell size could be taken as the fundamental particles, given the running nature of the coarse-graining length. Those “fundamental particles” have a larger  $\mathcal{M}_2$ , which could also be subtracted. In fact, if we had information of the distribution of stellar mass inside the galaxies, we could also reduce the cell size and so reduce the given “minimum” value of  $\mathcal{M}_2$ . Naturally, this reduction should extend the scaling range in the lower plot of Fig. 7 to smaller values of  $\Omega$ .

#### 5.4. Finding the scale $r_0$

The scale of homogeneity  $\Omega_0$  of the projected distribution can be found by solving the equation  $\mu_2(\Omega_0) - 1 = 1$ , according to Eq. (18). After finding  $\Omega_0$ , the scale of homogeneity of the three-dimensional distribution is found through

Eq. (16), by expressing the mass variance  $\mu_2(\Omega) - 1$  as the average of  $w(\theta)$ , so that  $\Omega_0$  is expressed in terms of  $r_0/d_*$ ,  $K$  and  $\gamma$ , which results in an equation for  $r_0/d_*$ . Finally,  $r_0$  is calculated after estimating  $d_*$ .

Let us work out the relation between  $\Omega_0$ ,  $r_0/d_*$ ,  $K$  and  $\gamma$ . From Eq. (16) and Eq. (18),

$$\begin{aligned} \Omega_0^{(\gamma-1)/2} &= \Omega^{(\gamma-1)/2} \int \frac{d\Omega_1 d\Omega_2}{\Omega^2} w(\theta_{12}) \\ &= K \left( \frac{r_0}{d_*} \right)^\gamma k_\gamma \int \frac{d\Omega_1 d\Omega_2}{\Omega^2} \left( \frac{\theta_{12}}{\Omega^{1/2}} \right)^{1-\gamma}, \end{aligned} \quad (20)$$

where  $k_\gamma$  is the integral in Eq. (16) and the integral over  $\Omega_1$  and  $\Omega_2$  extends over a cell. Given  $\gamma$ , the evaluation of  $k_\gamma$  and the integral over  $\Omega_1$  and  $\Omega_2$  are straightforward numerical computations (for this integral, we take into account the small size of the relevant cells, which allows us to ignore the spherical geometry and carry out the computation in the plane). To calculate the constant  $K$ , which is an integral that contains the luminosity function, we can use the Schechter model (Peebles 1993). This model has two parameters, but  $K$  only depends on one of them, namely, the slope  $\alpha$ , which we take as  $\alpha = -1.08$  (a reasonable value, although there is a certain variance, as studied by Zandivarez and Martínez 2011).

To solve for  $r_0/d_*$  we have to fix  $\gamma$  and  $\Omega_0$ . We proceed independently for the galaxy number and stellar mass distributions. We take the values of  $\gamma$  found in Sect. 5.3 and compute the values of  $\Omega_0$ . The computation of these values yields  $8.57 \cdot 10^{-7}$  and  $9.53 \cdot 10^{-7}$  steradians for the galaxy number and stellar mass distributions, respectively (they are close values).

Let us first consider the number distribution, with  $\gamma = 1.75$ . We obtain that  $k_\gamma = 3.86$ , the integral over  $\Omega_1$  and  $\Omega_2$  yields 2.11, and  $K = 1.01$ . Employing Eq. (20), we obtain

$$r_0/d_* = 0.0150.$$

Let us estimate the characteristic sample depth  $d_*$ . This depth is proportional to the square of the characteristic galaxy luminosity  $L_*$  and, hence, the estimation of  $d_*$  is the most uncertain step in the calculation of  $r_0$ . We take  $M_*$ , the absolute magnitude corresponding to  $L_*$ , to be

$$M_* - 5 \log_{10} h = -20.5;$$

but it has considerable variance (Zandivarez and Martínez 2011). We obtain

$$d_* = 10 \text{ pc} \times 10^{0.2(17.77+20.5-5 \log_{10} h)} = 450 \text{ Mpc}/h.$$

Therefore,

$$r_0 = 6.8 \text{ Mpc}/h.$$

The analogous calculation for the stellar mass distribution, with  $\gamma = 1.83$ , yields

$$r_0 = 5.9 \text{ Mpc}/h.$$

It agrees well with the value found by Li and White (2009).

We can also calculate the value of  $r_0$  given by the scaling of  $\mu_2(\Omega_0) - 1$  found in Sect. 5.1, before the shot noise suppression, with  $\gamma = 1.97$ . We obtain  $\Omega_0 = 4.39 \cdot 10^{-6}$ . Hence, we obtain

$$r_0 = 6.5 \text{ Mpc}/h.$$

Notice that this value is between the preceding ones, in spite of the fact that the value of  $\Omega_0$  is sensibly larger than the preceding values.

## 6. Fractional statistical moments

The angular analysis in the preceding section is based on the order two statistical moment  $\mu_2(\Omega)$  and, specifically, on the variance  $\mu_2(\Omega) - 1$ . A complete multifractal analysis requires the full set of  $q$ -moments  $\mu_q(\Omega)$ , Eq. (14). In fact, the “area-averaged angular correlations”  $\bar{\omega}_p(\theta)$  have been defined and studied for integral  $p$  (Bernardeau et al. 2009), and they are equivalent to  $\mu_p(\Omega)$  (assuming a 2d circular window of size  $\Omega$  and the reduction to irreducible components). However, the restriction to integral orders leads to a set of moments of little utility for us. On the one hand, integral order moments are not sufficient to characterize mass distributions with considerable probability of high densities, in particular, multifractal distributions (Coles and Jones 1992; Gaite 2007). On the other hand, we have to consider the restriction  $1 < q \leq 2$  for fractal projections (Sect. 3). Therefore, we consider here fractional order statistical moments in this interval.

Fractional order moments can have different properties from integral order moments. For example, we must notice, in regard to the shot noise suppression introduced in Sect. 3 for  $\mu_2(\Omega)$  and also possible for higher order integral moments, that it is not possible for fractional order moments with  $1 < q \leq 2$ . Let us recall that the shot noise suppression for  $\mu_2(\Omega)$  is achieved by just subtracting from  $\mathcal{M}_2$  its minimum value (for small scale  $l$ ). The minimum value of  $\mathcal{M}_q$  grows with decreasing  $q$  and, in fact, it reaches the value of one for  $q = 1$  ( $\mathcal{M}_1 = 1$  for any scale  $l$ ). This shows that the minimum value of  $\mathcal{M}_q$  cannot be subtracted when  $q \gtrsim 1$ , and therefore the “shot noise suppression” does not make sense in these cases.

For definiteness, let us consider  $q = 1.5$ , just in the middle of the interval  $[1, 2]$ , and calculate  $\mu_{1.5}(\Omega)$ . We do it in analogy to the calculation of  $\mu_2(\Omega)$  (in particular, with the restriction  $z < 0.34$ ). We know that  $\mu_q(\Omega)$  must be equal to one at the largest  $\Omega$  (the sample size) and, in fact,  $\mu_2(\Omega)$  approaches one for fairly small  $\Omega$ . Likewise,  $\mu_{1.5}(\Omega)$  approaches one for fairly small  $\Omega$ . Therefore, we calculate  $\mu_{1.5}(\Omega) - 1$ . First of all, we check that the subtraction from  $\mathcal{M}_{1.5}(\Omega)$  of its minimum value renders negative the values of  $\mu_{1.5}(\Omega) - 1$  in the full range of  $\Omega$ , proving that the “shot noise suppression” does not make sense already at  $q = 1.5$ , which is not too close to one. The log-log plot of  $\mu_{1.5}(\Omega) - 1$  (without shot noise subtraction) is displayed in Fig. 8. It is similar to the log-log plot of  $\mu_2(\Omega) - 1$  (in the upper plot in Fig. 5). The slope of the log-log plot of  $\mu_{1.5}(\Omega) - 1$  is  $-0.480 \pm 0.007$  (it is  $-0.486 \pm 0.008$  for  $\mu_2 - 1$ ). The values of  $\mu_{1.5}(\Omega) - 1$  are somewhat smaller than the ones of  $\mu_2(\Omega) - 1$ .

The scaling exponent of  $\mu_q(\Omega)$  gives the dimension spectrum  $D_q$ , according to Eq. (15). It is evident that we cannot obtain  $D_{1.5}$  from the slope of the log-log plot of  $\mu_{1.5}(\Omega) - 1$ , because the scaling range of  $\mu_{1.5}(\Omega) - 1$  occurs where  $\mu_{1.5}(\Omega) \simeq 1$ , and  $\mu_{1.5}(\Omega)$  itself does not scale (indeed, the value of  $D_{1.5}$  that Eq. (15) would yield is absurd). However, we can employ a model for the mass distribution that interpolates between the nonlinear and linear cosmological regimes and, therefore, covers the full range of scales. A model that achieves that and is furthermore consistent with the multifractal model is the lognormal model (Coles and Jones 1992). For this model,

$$\mu_q = e^{q(q-1)\sigma^2/2},$$

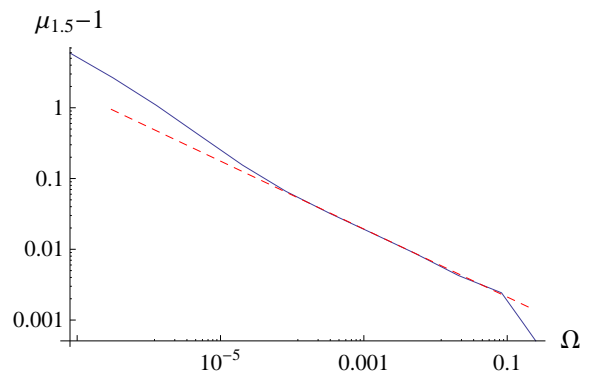


**Fig. 8.** Log-log plot of  $\mu_{1.5}(\Omega) - 1$  for the stellar mass, with linear fit.

where the variance of the underlying normal distribution  $\sigma^2$  is a scale dependent magnitude. The lognormal model is a model of the three-dimensional mass distribution but it can also be applied to its angular projection; and then  $\mu_q(\Omega)$  depends on  $\sigma^2(\Omega)$ . We have, in particular,

$$\mu_2 = e^{\sigma^2}, \quad \mu_{3/2} = e^{3\sigma^2/8}.$$

For a quasi-uniform mass distribution of this type,  $\sigma^2 \ll 1$  and

$$\mu_2 - 1 \approx \sigma^2, \quad \mu_{3/2} - 1 \approx 3\sigma^2/8.$$

This amounts to a constant ratio

$$\frac{\mu_{3/2} - 1}{\mu_2 - 1} \approx \frac{3}{8} = 0.375.$$

Given that the power-law exponent that we have obtained for  $\mu_{3/2} - 1$  is slightly smaller in absolute value than the exponent for  $\mu_2 - 1$ , we have a ratio that slightly increases with  $\Omega$ , starting at 0.363 for  $\Omega = 10^{-4}$  and reaching 0.376 for  $\Omega = 5 \cdot 10^{-2}$ . These values are in good accord with the lognormal model prediction.

This analysis confirms that the projected mass distribution obtained from our sample only gives information of the quasi-linear cosmological regime, while the scaling in the nonlinear regime is not represented (in the lognormal model, this regime corresponds to  $\sigma^2 \gg 1$ ). Indeed, the nonlinear scaling should appear for very small values of  $\Omega$ , where the moments  $\mu_q(\Omega)$  are too influenced by discreteness effects.

In spite of the fact that the analysis of  $q$ -moments does not give access to truly fractal properties, it is valid for establishing the transition to homogeneity. The condition for the transition to homogeneity of the projected mass distribution that we have employed, namely,  $\mu_2(\Omega_0) - 1 = 1$ , can be generalized to all  $q$  as  $\mu_q(\Omega_0) = 2$ . However, different values of  $q$  will not give the same value of  $\Omega_0$ . This is shown, in particular, by the lognormal model. The expression of  $\mu_q$  yields

$$\sigma^2(\Omega_0) = \frac{2 \ln 2}{q(q-1)}.$$

That is to say, the value of  $\sigma^2$  at the transition to homogeneity decreases if calculated for larger  $q$ , and, therefore, the value of  $\Omega_0$  increases (naturally,  $\sigma^2(\Omega)$  is a monotonically decreasing function). At any rate, the values of the three-dimensional scale  $r_0$ , calculated from  $\mu_2$  in Sect. 5, are convenient to establish the scale of the transition to homogeneity in this sample.

## 7. Conclusions and discussion

The general conclusion is, of course, that the angular projection of the distribution of stellar mass reveals features not seen in the distribution of individual galaxies (the galaxy number distribution). These new features are worth considering.

The stellar mass distribution is a proxy for the distribution of baryonic matter (in spite of the fact that most baryons are not in stars). The scaling properties of the stellar mass distribution are very relevant because they are expected to be quite similar to those of the dark matter distribution. Indeed, Li and White (2009) show that the bias of the stellar mass relative to the dark matter in  $w(r_p)$  is approximately constant for  $r_p > 1.5 h^{-1}\text{Mpc}$ . Furthermore, Gaite (2018) shows that the multifractal spectrum of the stellar mass obtained from SDSS-DR7 volume limited samples and the multifractal spectrum of the dark matter distributions obtained from  $N$ -body simulations are fully compatible.

The standard scaling law of galaxy clustering is the power-law correlation function with canonical exponent  $\gamma = 1.8$  and clustering length  $r_0 \simeq 5 h^{-1}\text{Mpc}$ , which has been hardly altered for 50 years, since the early analyses of the galaxy-galaxy angular correlation function. The largest scaling ranges are still obtained with this method. In particular, the recent analysis of the angular correlation function by Wang, Brunner and Dolence (2013) achieves an impressive scaling range and essentially agrees with the standard law. Li and White' analysis of the projected correlation function  $w(r_p)$  of stellar mass achieves an equally good scaling range and also agrees with the standard law.

Our study is based on multifractal geometry, in which the correlation dimension  $D_2 = 3 - \gamma$  is only one of the many dimensions  $D_q$  that can be measured and not the most significant one. However, it is the only integral dimension that can be measured from the angular projection of the stellar mass distribution, in principle, because there is only a small subinterval  $[q, 2]$  of  $[1, 2]$  where  $D_q$  is given by the projection, as shown in Sects. 3 and 4. In our analysis of the projected distribution, we achieve good scaling ranges for  $\mu_2(\Omega) - 1 = (\delta M_\Omega / M_\Omega)^2$ , equivalent to the angular correlation function  $w(\theta)$ , and for  $\mu_q(\Omega) - 1$  with  $q = 1.5$  (selected from  $q \in [1, 2]$ ). For example, in the lower plot of Fig. 3, the scaling range is a factor of 4096 in  $\Omega$ , equivalent to a factor of 64 in the angle  $\theta$ , while the ranges in Fig. 5 are a bit smaller. Our first analysis, which takes the full magnitude-limited sample, shows that the angular correlation function of the projected stellar mass distribution obtained from a magnitude-limited sample is dominated by a small number of large and isolated masses and, therefore, has  $\gamma = 3$  ( $D_2 = 0$ ). This effect is due to the excess of massive galaxies at high redshift. In fact, by removing the small number of galaxies with  $z > 0.34$ , we recover a power law with a reasonable value of  $\gamma$ , namely,  $\gamma = 1.97$ . However, this value is larger than the value  $\gamma = 1.83$  that we obtain without the galaxy masses.

To compare with the results of Li and White (2009) for the stellar mass distribution or the results of Wang, Brunner and Dolence (2013) for the galaxy number distribution, we suppress the shot noise that arises in any mass distribution that consists of particles. We obtain  $\gamma = 1.83$  and  $r_0 = 5.9 h^{-1}\text{Mpc}$ , for the stellar mass distribution, and  $\gamma = 1.75$  and  $r_0 = 6.8 h^{-1}\text{Mpc}$ ,

for the galaxy number distribution, in good agreement (Wang, Brunner and Dolence do not determine  $r_0$ ). If we compare the scalings of the stellar mass and galaxy distributions (Fig. 7), we find that the former is better, as do Li and White.

At any rate, we argue that the suppression of shot noise may not be meaningful for the stellar mass distribution, because the condensation of stellar mass into point-like galaxies is artificial and is not suitable for a proper statistical analysis with a running scale, such as our multifractal analysis is. Indeed, we show that one runs into problems when one attempts to subtract the shot noise term from fractional statistical moments, especially, the moments with  $q \gtrsim 1$ . Of course, discreteness effects are present in the multifractal analysis of any mass distribution that consists of particles, but a simple subtraction is surely not a suitable way to correct for them.

We must emphasize that the various versions of a scaling law that we have found and quoted above occur for small values of  $\delta M/M$  (or  $\delta N/N$ ) (except in the case of the preliminary result with  $\gamma = 3$ ). Therefore, they correspond to a projection that is quasi-homogeneous and not fractal. Unfortunately, a precision value of  $\gamma$  found in the quasi-homogeneous regime does not determine  $D_2$  or any fractal property. However, we can also set a low redshift cutoff, for example,  $z = 0.025$ , which removes the majority of galaxies and allows us to probe the strong clustering regime,  $\delta M \gg M$ . Indeed, the cosmic web structure is preserved in the projection. Therefore, we have access to fractal properties and we can speak of the correlation dimension, which is calculated as  $D_2 = 3 - \gamma$ . The power law fit of the scaling of  $\delta M/M$  yields  $\gamma \simeq 2$ , as in the case of the  $z = 0.34$  cutoff, but now with a scaling range in the strong clustering regime. However, this range is hardly sufficient and the scaling of the full second statistical moment  $\mu_2(\Omega)$  only obtains an uncertain  $D_2 \in (1, 1.2)$ .

In principle, there is nothing wrong even with  $D_2 = 1$ , but coherence with previous multifractal analyses demands that  $D_2 > 1$ . Indeed, the multifractal analyses of the stellar mass distribution in SDSS-DR7 and of the dark matter distribution in cosmological simulations show that the minimum value of the local dimension is  $\alpha_{\min} = 1$ , that is to say, the value at which the gravitational potential diverges (Gaite 2018, 2019). On the other hand, it is easy to prove, for a general multifractal, that  $D_q > \alpha(q)$ , if  $q > 1$ . Therefore,  $D_2 > \alpha(2) > \alpha_{\min} = 1$ , in this case.

The  $z < 0.025$  sample comprises a portion of the local universe, with a linear size that is not much larger than the linear size of the volume-limited sample VLS1 (Sect. 2) or the range  $r_p < 30 h^{-1}\text{Mpc}$  of Li and White (2009). The scaling of  $\delta M/M$  in the former and the scaling of  $w(r_p)$  in the latter both yield values of  $\gamma$  close to the standard value  $\gamma = 1.8$  deduced from the galaxy number distribution. As regards the scaling range of VLS1 in the strong clustering regime, it is small, so the value  $D_2 = 1.2$  is uncertain and actually we can only say that  $D_2 \in (1.2, 1.4)$  [whereas the range obtained from the  $z < 0.025$  sample is  $D_2 \in (1, 1.2)$ ]. The part of the scaling range of Li and White that is in the strong clustering regime is difficult to know, so one cannot determine the consequent uncertainty in the value of  $D_2$ . We have already pointed out in the introduction the problems with the projected correlation function  $w(r_p)$ . It is defined by integration of the standard two-point correlation function over the coordinate  $\pi$  perpendicular to the

line of sight, giving a dimensional function. In fact, the integration over  $\pi$  in  $(-\infty, \infty)$  does not seem to be meaningful, because the integral of the full correlation function  $1 + \xi$  over  $\pi$  in  $(-\infty, \infty)$  is divergent. The integration over  $\pi$  is restricted to a finite interval, somewhat arbitrarily: Li and White (2009) set  $|\pi| < 40 h^{-1} \text{Mpc}$  for the limitation of noise. The inevitable arbitrariness in the range of  $\pi$  underscores the questionable conceptual nature of  $w(r_p)$ .

Our general conclusion is that the study of the projected stellar mass distribution is not especially useful to determine the fractal geometry of the large scale structure, although our brief study of fractional moments supports the lognormal model and hence the multifractal character of the distribution. At any rate, our study is useful to fix the scale of transition to homogeneity. If this scale is defined in terms of the two-point correlation function, the values that we obtain in Sect. 5.4, for the galaxy number distribution or the stellar mass distribution with or without shot-noise suppression are quite close and, in turn, close to the standard value  $r_0 \simeq 5 h^{-1} \text{Mpc}$ . The error is not in the one percent level that some calculations of  $\sigma_8$  purport to achieve but is quite moderate, in spite of the fact that the calculation of  $r_0$  from the projected distribution is subject to considerable uncertainties (for example, in the luminosity function). The calculation of  $r_0$  from volume limited samples could give a more accurate value, in principle, but is hindered by the problem of making suitable volume limited samples. In particular, the absence of massive galaxies in these samples is a problem when we consider the stellar mass distribution.

As said in the introduction, the range of values of the scale of transition to homogeneity in the literature is very ample. This is due, in part, to the various definitions of this scale that have been used. The scale  $r_0$  is well defined if we consider a definite power-law two-point correlation function, but there are definitions of the scale transition to homogeneity based on other magnitudes. As regards the fractal geometry, we have pointed out in Sect. 6 that one can use any fractional statistical moment to define the scale of transition to homogeneity and that the scale depends on the fractional statistical moment used. From the standpoint of fractal geometry, values of  $q$  close to one should be preferable. It is pertinent to mention that several authors that have carried out multifractal analysis of the galaxy number distribution have used criteria of convergence of the dimensions to their homogeneity values, and that they tend to obtain large values of the scale of transition to homogeneity. Surely, it is better to use the stellar mass distribution and a criterion based on the behaviour of statistical moments.

To recapitulate, we have observed that the presence of very massive galaxies makes the statistical analysis of the stellar mass distribution more subtle than the analysis of the mere galaxy number distribution. Indeed, a very small number of very massive galaxies can rule the behaviour of the correlation function and actually determine a correlation dimension  $D_2 = 0$  and an extremely large scale of transition to homogeneity. This effect can be corrected, thus obtaining values of these quantities in accord with the standard values obtained from the galaxy number distribution. However, the broad range of galaxy masses still makes the statistical analysis more involved. For example, we have to consider that the more suitable volume-limited samples only cover a range of small masses and that the method ap-

plied to the angular distribution involves the use of galaxy redshifts and some assumptions. These problems may have consequences for current methods of calculating precision values of  $\sigma_8$ .

## Acknowledgements

I thank C.A. Chacón-Cardona for the SDSS-DR7 file.

## References

- Abazajian K.N. et al, *The Seventh Data Release of the Sloan Digital Sky Survey*, *ApJS* **182** (2009) 543–558.
- Bernardeau F., S. Colombi, E. Gaztañaga and R. Scoccimarro, *Large-scale structure of the Universe and cosmological perturbation theory*, *Phys. Rep.* **367** (2002) 1–248.
- Blanton M.R. et al, *New York University Value-Added Galaxy Catalog: A Galaxy Catalog Based on New Public Surveys*, *AJ* **129** (2005) 2562–2578.  
<http://sdss.physics.nyu.edu/vagc> NYU Value-Added Galaxy Catalog web page.
- Blanton M.R. and S. Roweis, *K-Corrections and Filter Transformations in the Ultraviolet, Optical, and Near-Infrared*, *AJ* **133** (2007) 734–754.
- Chacón-Cardona C.A., R.A. Casas-Miranda, J.C. Muñoz-Cuartas, *Multi-fractal analysis and lacunarity spectrum of the dark matter haloes in the SDSS-DR7, Chaos, Solitons and Fractals* **82** (2016) 22–33.
- Coleman P.H. and L. Pietronero, *The fractal structure of the Universe*, *Phys. Rep.* **213** (1992) 311–389.
- Coles P. and B.J. Jones, *A lognormal model for the cosmological mass distribution*, *MNRAS* **248** (1991) 1–13.
- Davis, M., Peebles, P.J.E., *A survey of galaxy redshifts. V - The two-point position and velocity correlations*, *Astrophys. J.* **267** (1983) 465–482.
- DES Collaboration: Abbott et al., *Dark Energy Survey Year 1 Results: Cosmological Constraints from Galaxy Clustering and Weak Lensing*, *Phys. Rev. D* **98** 043526 (2018).
- Durrer R., J.-P. Eckmann, F. Sylos Labini, M. Montuori and L. Pietronero, *Angular Projections of Fractal Sets*, *Europhysics Letters* **40** (1997) 491–496.
- Falconer K., *Fractal Geometry (Second Edition)*, John Wiley and Sons, Chichester, UK, (2003).
- Falconer K., J.M. Fraser and Xiong Jin, *Sixty years of fractal projections, in Fractal Geometry and Stochastics V, Progress in Probability* **70**, Birkhauser (2015), pg. 3–25 [arXiv:1411.3156].
- Gaite J., *Halos and voids in a multifractal model of cosmic structure*, *Astrophys. J.* **658** (2007) 11–24.
- Gaite J., *Fractal analysis of the large-scale stellar mass distribution in the Sloan Digital Sky Survey*, *JCAP* **2018**, 07, 010.
- Gaite J., *The Fractal Geometry of the Cosmic Web and Its Formation*, *Advances in Astronomy* **2019**, Article ID 6587138, 25 pages. <https://doi.org/10.1155/2019/6587138>.
- Gaite J., A. Domínguez and J. Pérez-Mercader, *The fractal distribution of galaxies and the transition to homogeneity*, *Astrophys. J.* **522** (1999) L5–L8.
- Geller M.J. and J.P. Huchra, *Mapping the Universe*, *Science* **246** (1989) 897–903.
- Groth E.J. and P.J.E. Peebles, *Statistical analysis of catalogs of extragalactic objects. VII - Two- and three-point correlation functions for the high-resolution Shane-Wirtanen catalog of galaxies*, *Astrophys. J.* **217** (1977) 385–405.
- Harte D., *Multifractals. Theory and applications*, Chapman & Hall/CRC, Boca Raton, Fla. (2001).
- Hunt B.R. and V.Y. Kaloshin, *How projections affect the dimension spectrum of fractal measures*, *Nonlinearity* **10** (1997) 1031–1046.
- Jones B.J.T., *Precision Cosmology: The First Half Million Years*, Cambridge University Press (2017).
- Jones B.J.T., V. Martínez, E. Saar and V. Trimble, *Scaling laws in the distribution of galaxies*, *Rev. Mod. Phys.* **76** (2004) 1211–1266.
- Kauffmann G. et al, *Stellar Masses and Star Formation Histories for  $10^5$  Galaxies from the Sloan Digital Sky Survey*, *MNRAS* **341** (2003) 33–53.
- Kofman L., D. Pogosyan, S.F. Shandarin and A.L. Melott, *Coherent structures in the universe and the adhesion model*, *The Astrophysical Journal* **393** (1992) 437–449.

- Lahav O. and A.R. Liddle, *The Cosmological Parameters*, in C. Patrignani *et al.* (Particle Data Group), *Chin. Phys. C* **40** (2016) [2017 update] 100001.
- Li Ch. and S.D.M. White, *The distribution of stellar mass in the low-redshift Universe*, *MNRAS* **398** (2009) 2177–2187.
- Mandelbrot B.B., *The fractal geometry of nature* (rev. ed. of: *Fractals*, 1977), W.H. Freeman and Company (1983).
- Peebles P.J.E., *Principles of Physical Cosmology*, Princeton University Press (1993).
- Pietronero L., *The fractal structure of the universe: Correlations of galaxies and clusters and the average mass density*, *Physica A* **144** (1987) 257–284.
- Sarkar P., J. Yadav, B Pandey and S. Bharadwaj, *The scale of homogeneity of the galaxy distribution in SDSS DR6*, *MNRAS* **399** (2009) L128–31.
- Sylos Labini F., M. Montuori and L. Pietronero, *Scale invariance of galaxy clustering*, *Phys. Rep.* **293** (1998) 61–226.
- Sylos Labini F., NL Vasilyev and YV Baryshev, *Power law correlations in galaxy distribution and finite volume effects from the Sloan Digital Sky Survey Data Release Four*, *Astron. Astrophys.* **465** (2007) 23–33.
- Totsuji H. and T. Kihara, *The Correlation Function for the Distribution of Galaxies*, *Publ. Astron. Soc. Japan* **21** (1969) 221.
- Verevkin A.O., Y.L. Bukhmastova and Y.V. Baryshev, *The non-uniform distribution of galaxies from data of the SDSS DR7 survey*, *Astron Rep* **55** (2011) 324–40.
- Wang Y., R.J. Brunner and J.C. Dolence, *The SDSS galaxy angular two-point correlation function*, *MNRAS* **432** (2013) 1961–1979.
- Zandivarez A. and H.J. Martínez, *Luminosity function of galaxies in groups in the Sloan Digital Sky Survey Data Release 7: the dependence on mass, environment and galaxy type*, *MNRAS* **415** (2011) 2553–2565.